PCCP

ROYAL SOCIETY OF CHEMISTRY

PAPER

View Article Online
View Journal | View Issue

Cite this: *Phys. Chem. Chem. Phys.*, 2024, **26**, 22593

An innovative deep eutectic solvent: chalcogen bonding as the primary driving force†

Ruifen Shi,[b] Zeyu Wang,[a] Dongkun Yu,*[c] Chenyang Wei,[a] Rui Qin[a] and Tiancheng Mu *[ad]

Received 6th April 2024,
Accepted 4th August 2024

DOI: 10.1039/d4cp01419g

rsc.li/pccp

Chalcogen bonding (ChB) interactions have drawn intensive attention in the last few decades as interesting alternatives to hydrogen bonding. The applications of ChB were mostly centered on the solid state and have rarely been explored in solution. In this work, a novel strategy for forming ChB-based deep eutectic solvents (DESs) was exploited. We set forth the formation, physicochemical properties, and interaction sites in detail. This work not only provides a new idea to design DES systems but also to exploit the potential application of ChB complexes.

Introduction

Deep eutectic solvents (DESs), an emerging system of green solvents, are easily available, potentially extensible, low cost and eco-friendly.[1,2] DESs typically consist of at least two components, including a hydrogen bond donor (HBD) and hydrogen bond acceptor (HBA), exhibiting a reduced melting point observably below those of pure components.[3] Given the feature of high design freedom, DESs have been widely employed in different applications, such as dissolution and extraction,[4] materials chemistry,[5] biomass treatment,[6] and organic synthesis.[7] Nevertheless, the further expansion of DESs faces a major bottleneck of being restricted to hydrogen bonding interaction as the only formative force to form eutectic systems. As a result, it is essential to exploit a new DES system driven by other noncovalent interactions such as halogen bonding (XB)[8] and chalcogen bonding.

ChB, a highly efficient and versatile non-covalent bond, known as the ''sister'' of halogen bonding, has attracted substantial attention from scientific communities.[9] It is an attractive interaction between electrophilic sulfur substituents (Ch; S, Se, and Te) and electron-donor Lewis bases, denoted as R-Ch-LB, which is also a type of σ-hole interaction, with the σ-hole located in the positive electrostatic potential region along the extension of the R-Ch axis.[9] Theoretical calculations have revealed a lot of similarities between ChB and XB. However, XB is formed with only one σ-hole at the end of the X atom, whereas for ChB, there may be one or two σ-holes around Ch, both of which may form ChB interactions with LB.[10] Owing to the presence of the σ-hole, ChB interaction is highly directional. In view of its unique advantages, it has been applied to different fields, including anion recognition, organocatalysis, crystal processing, and biological applications.[11–14] However, current studies on ChB are fundamentally based on crystallographic and intramolecular/intermolecular theoretical calculations, and reports regarding ChB interactions in solution are lacking. There still remains a gap in the exploration of unprecedented applications of ChB.

The field of DESs is developing, and various new concepts have been proposed, such as Type V DESs. These non-ionic DESs were prepared based on the abnormally strong interaction caused by the difference in acidity between phenolic hydroxyl and aliphatic hydroxyl.[15] Eutectic molecular liquids have expanded the types of interactions and attracted the attention of researchers.[16] Additionally, inverted DESs were defined and their physicochemical and electrochemical properties were studied.[17] The host–guest interaction based on potassium ions makes it possible to use inverted DESs as an electrolyte for potassium ion batteries. On the one hand, progress has been made in both non-covalent interactions and eutectic solvents. On the other hand, the correlation between the two makes us think about establishing a connection between them.

In 2017, Zhang *et al.* reported that σ-hole interactions can be utilized to stabilize unstable anions, just like hydrogen bonding interactions.[2] Zhang's work is inspiring. It is well known that a conventional DES is based on hydrogen bond interactions. Can ChB interactions also help form a eutectic system? The answer

[a] *School of Chemistry and Life Resources, Renmin University of China, Beijing 100872, China. E-mail: tcmu@ruc.edu.cn; Tel: +86-10-62514925*
[b] *Zhejiang Institute of Mechanical and Electrical Engineering Corporation Limited, Hangzhou 310051, China*
[c] *Department of Applied Physics, KTH Royal Institute of Technology, Hannes Alfvéns väg 12, 11419, Stockholm, Sweden*
[d] *School of Chemistry and Chemical Engineering, Henan Normal University, Xinxiang, Henan 453007, China*

† Electronic supplementary information (ESI) available. See DOI: https://doi.org/10.1039/d4cp01419g

is ''yes''. Herein, we designed and synthesized ChB-based DESs for the first time. Then, the eutectic systems were characterized by UV-vis, FT-IR and nuclear magnetic resonance (NMR) spectroscopy. The thermal properties were investigated by thermogravimetric analysis (TGA) and differential scanning calorimetry (DSC). Theoretical calculations were applied to demonstrate the strong ChB interaction between the donor and the acceptor. This work not only unlocks the feasibility of ChB interactions in the application of solvents but provides an original idea to design more types of DESs.

Experimental

Materials

Tetrabutylammonium chloride (TBAC, 98%) was obtained from Saen Chemical Technology Co., Ltd (Shanghai, China). Tetrabutylammonium bromide (TBAB, 99%) was acquired from Adamas Reagent Co., Ltd. Phenylselenium bromide (PhSeBr, 98%) and phenylselenium chloride (PhSeCl, 95%) were obtained from Macklin Biochemical Co., Ltd (Shanghai, China). All chemicals were used as received without further purification.

Synthesis

All ChB DESs were obtained by mixing the ChB donors and acceptors in appropriate molar ratio and then heating and stirring at a preset temperature. The heating temperature was set to 80 °C for the mixtures based on TBAB and PhSeBr/PhSeCl and 70 °C for the mixtures based on TBAC and PhSeBr/PhSeCl. All the mixtures were mixed at 400 rpm for 1 h until a homogeneous and stable clear brown/light yellow liquid was formed and then stored in a closed container at room temperature. Due to the hygroscopicity of the quaternary ammonium salts, both TBAB and TBAC needed to be dried in a vacuum oven before use, and the water content in the prepared ChB DESs was determined to be less than 100 ppm by Karl Fischer titration.

Characterization

DSC was carried out with a DSC Q200 (TA Instruments, USA) in a nitrogen atmosphere at a ramp rate of 5 °C min^{-1}. All eutectic solvents were placed in a sealed aluminium crucible, cooled to −60 °C and then heated to room temperature, and the equipment was calibrated in this temperature range. FT-IR spectra were recorded on a Bruker Tensor 27 infrared spectrometer, and the samples were prepared using the KBr sheet method in the range from 500 to 4000 cm^{-1}. Dynamic infrared spectroscopy was carried out in a closed and anhydrous environment. UV-vis absorption spectra were recorded using a spectrophotometer (UV-3600, Shimadzu, Corp., Japan). The ^{13}C NMR experiments were tested on a Bruker Avance 400 MHz spectrometer. TGA curves were obtained by a TGA Q4000 (PerkinElmer Instruments Inc.) in the 10 °C min^{-1} ramp mode under nitrogen atmosphere.

The molecular structures of ChB DESs were further investigated using density functional theory (DFT) calculations, built with the Gaussview 5.0 program and then optimized with Gaussian 09. M06-2X was chosen as the general function and def2-SVP as the basis set for optimizing the structures. The interaction energy (E_{int}) of complex A–B was calculated by the equation $E_{int} = E(AB) - E(A) - E(B)$. The minimum and maximum values of the electrostatic potential on the surface of the ChB donor ($V_{s,min}$ and $V_{s,max}$, respectively) were calculated using Multiwfn. For the RDG-based calculations, the NCI spike values and corresponding isosurface plots were generated by combining the Multiwfn results with VMD. In addition, the bond critical point (BCP) of ChB was found using Multiwfn and detailed topological and orbital analyses were carried out as well.

Results and discussion

Design of ChB DES systems

The halide anions are typical Lewis bases possessing unparalleled characteristics, such as small steric hindrance, large charge density and radius, high polarizability and multi-coordination numbers. Most importantly, they present simple electronic and vibrational spectra, which are beneficial for the research on noncovalent interactions.[18] On the other hand, the ChB donor (typically, a molecular compound) must have at least one chalcogen atom center whose steric hindrance should not be too large. Furthermore, there shall be electron-withdrawing atoms or functional group bonding to the chalcogen atom to raise a positively charged σ-hole. Therefore, we chose quaternary ammonium salts as the ChB acceptors, and phenyl selenium bromide (PhSeBr) and phenyl selenium chloride (PhSeCl) were used as the ChB donors in this work, obtaining four types of chalcogen bonding-based DESs (ChB DESs for short) by modulating the components and ratios.

A molecular electrostatic surface potential

The electrostatic potential $V(r)$ is an efficacious tool to reflect the specific properties of a molecule and predict its reactive behavior, particularly in noncovalent interactions.[19] In view of

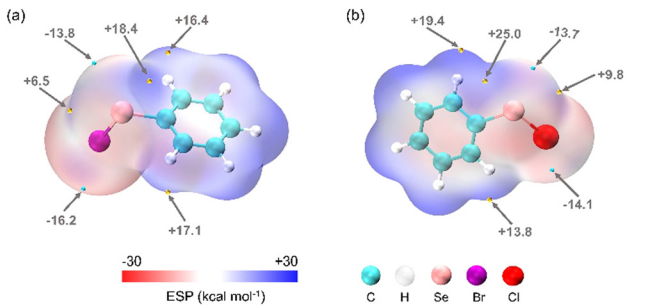

Fig. 1 Molecular electrostatic potential surface of (a) PhSeBr and (b) PhSeCl computed at the M06-2X/def2-SVP level and plotted at 0.001 a.u. electron density contours. The cyan and yellow spheres where arrows point correspond to the most negative and positive regions of electrostatic potential on the molecule surface, respectively.

this, we displayed the electrostatic potential plots of ChB donors in Fig. 1, and those for ChB acceptors can be seen in our previous work.[8] We could clearly see that PhSeBr and PhSeCl both present two different σ-holes around the center of respective Se atoms, with one σ-hole located on the reverse extension of the Se–C bond and the other σ-hole located on the reverse extension of the Se–Br/Cl bond. From the overall electrostatic potential distribution, the σ-holes at Se atoms possess the largest $V_{s,max}$ values, and due to the strong electron-withdrawing nature of Cl atom, it makes the σ-hole at Se–Cl larger than Se–Br. Also, there still exists a negative potential region around the Se atom owing to its anisotropy.[20] For ChB acceptors, there is a large $V_{s,min}$ on the terminus of Cl^-/Br^-. From these, it seems clear that an electrostatic attraction might exist between the σ-hole of the Se atom and the halide anion of quaternary ammonium salt. By extension, as can be readily seen from the plots of the Laplacian of the electron density ($\nabla^2\rho$), the Se atoms are in a "naked" state, showing that they are easily attracted by nucleophiles (Fig. S1, ESI†). Thus, it can be concluded that an electrostatic attraction exists between the σ-hole of Se atom and Cl^-/Br^-.

Experimental characterization

Differential scanning calorimetry analysis was applied to better understand the thermal behavior of DESs. We present the melting points of the prepared ChB systems based on the whole range of TBAC/TBAB mol% (as shown in Fig. 2a and Fig. S2, ESI†). As expected, there was a significant melting point depression when the donor and acceptor were combined in different molar ratios, and the corresponding eutectic temperatures are provided in Table 1. Next, in order to clearly elucidate the formation mechanism of these DESs, we will focus on the

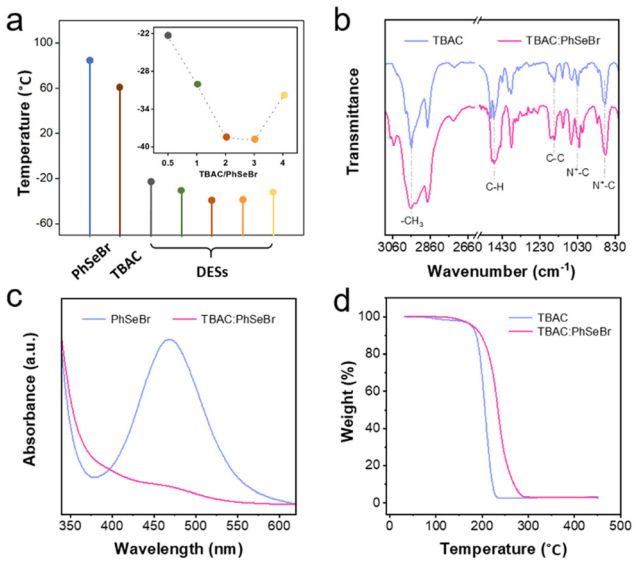

Fig. 2 (a) The melting points of PhSeBr, TBAC and DESs with different molar ratios. (b) The FT-IR spectra of pure TBAC and $(TBAC)_{0.5}(PhSeBr)_{0.5}$. (c) Normalized UV-vis spectra of pure PhSeBr and $(TBAC)_{0.5}(PhSeBr)_{0.5}$. The solvent is CH_2Cl_2. (d) TGA curves of pure TBAC and $(TBAC)_{0.5}(PhSeBr)_{0.5}$.

Table 1 The eutectic compositions and temperatures of ChB DESs

ChB donor	ChB acceptor	Mol% PhSeBr/PhSeCl	Eutectic temperature (°C)
PhSeBr	TBAC	25	−35.9
	TBAB	20	−39.2
PhSeCl	TBAC	25	−42.5
	TBAB	80	−38.2

eutectic systems with a molar ratio of 1 : 1. As illustrated in Fig. S3 (ESI†), a repeatable thermal behavior appeared in the successive cooling and heating cycles, showing that there was no chemical reaction between the parent components.[21] Besides, ^{13}C NMR spectroscopy displayed that the characteristic peaks of ChB DESs are basically consistent with that of pure acceptors without apparent shifts, indicating that only noncovalent interactions existed (Fig. S4, ESI†). Considering the above discussion, a eutectic system could be formed between the selected donors and acceptors.

Furthermore, we used infrared (IR) spectroscopy to further explore the intermolecular interactions of ChB complexes. As demonstrated above, it is possible that a ChB interaction exists between the Se atom and Cl^-/Br^-, and then we presented the IR spectra of the acceptors and corresponding complexes since the attribution of the C–Se stretching vibration of the donors is still in dispute.[22] In Fig. 2b, the IR spectrum of $(TBAC)_{0.5}(PhSeBr)_{0.5}$ is in accordance with that of pure TBAC as a whole, indicating that there are only noncovalent interactions between TBAC and PhSeBr. In detail, the characteristic peaks at 1031 cm^{-1} and 887 cm^{-1} both correspond to the N^+–C stretching vibration of TBAC.[23,24] When PhSeBr was added, the adsorption peaks of N^+–C exhibited red shifts while the other characteristic peaks remained same as that in the monomer, indicating that noncovalent interactions exist between Cl^- and PhSeBr. This arises from the fact that the vibrational bands of N^+R_4 are highly susceptible to Cl^-. The addition of PhSeBr will disrupt the intrinsic anion-cation interactions within TBAC, which influences the force constant of the N^+–C stretching mode, thus leading to red shifts of the N^+–C peaks in the complex.[25,26] Similar results could be seen for other ChB systems (Fig. S5, ESI†), and the details are listed in Table S1 (ESI†). Based on the above discussion, it could be concluded that ChB interaction exists between PhSeBr/PhSeCl and halide anions.

UV-vis absorption spectroscopy is typically used to prove the formation of ChB interactions as an effective tool.[11,27] Herein, we chose CH_2Cl_2 as a solvent owing to its good solubility and negligible effects.[28] As presented in Fig. 2c and Fig. S6 (ESI†), the pure components PhSeBr and PhSeCl showed characteristic absorption peaks at 468 nm and 432 nm, respectively, because of the auxochrome of selenium bromide and selenium chloride. As a representative, in the $(TBAC)_{0.5}(PhSeBr)_{0.5}$ system, the corresponding characteristic absorption was reduced by 89% owing to the strong interactions of Cl^- and Se–Br following the complexation with TBAC, which suppressed the chromogenesis.[29] Similarly, the reduction of all the characteristic absorption peaks could be observed in other ChB systems. From the above, it seems clear that

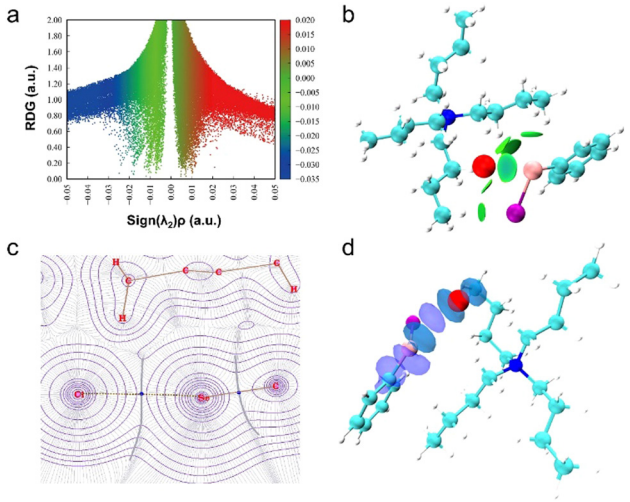

Fig. 3 (a) The plot of the reduced density gradient (RDG) *versus* the electron density multiplied by the sign of the second Hessian eigenvalue (sign(λ_2)ρ) and (b) the corresponding NCI isosurfaces (isovalue = 0.4 a.u.) of $(TBAC)_{0.5}(PhSeBr)_{0.5}$. (c) Gradient vector field of the electron density for Se···Cl^- interaction in $(TBAC)_{0.5}(PhSeBr)_{0.5}$; bond paths are shown as brown lines, bcps as dark blue, nuclear attractors as pink and interbasin paths as gray. (d) The plot of electron deformation density (isodensity surfaces correspond to the value of ± 0.002 a.u.; positive: purple and negative: blue). The coloured spheres represent different atoms, same as that in Fig. 1.

the formation of these eutectic mixture was driven by the ChB interaction between the components.

Then, we employed TGA analysis to further analyse the thermal behaviour of the prepared ChB DESs (see Fig. 2d and Fig. S7, ESI†). It is clear that these four eutectic systems all shower a higher T_{onset} value than the respective acceptor molecules,[8] indicating that a stronger ChB interaction was formed between the components and thus enhanced the thermostability of the eutectic complex. In addition, the ΔT_{onset} values between TBAC and the corresponding ChB DESs are higher than the other two related to the strong electron-withdrawing nature of Cl^- in TBAC. On the whole, the prepared ChB DESs possess better thermostability as solvents.

DFT calculations

To further comprehend and support the above viewpoints, the noncovalent interaction-reduced density gradient (NCI-RDG) serves as a powerful tool for the visualization of the regions in real space where weak interactions occur and the distinction of the types of interactions.[30] The NCI descriptor was constructed based on RDG as a function of sign(λ^2)ρ, the latter of which is beneficial to predict the nature of interactions and the values of >-0.025 a.u., -0.025 to -0.001 a.u., -0.001–0.001 a.u., and $>$ 0.001 a.u. are seen for partial-covalent, strong noncovalent interactions, van der Waals, and repulsive steric interactions, respectively.[31] From the NCI scatter plots of the four ChB systems (Fig. 3a and Fig. S8–S10a, ESI†), we could see that they all show a spike in the low-density and low-gradient region, indicating the existence of strong noncovalent interactions between the components of all the systems.[32] By comparison, the spike of the $(TBAC)_{0.5}(PhSeCl)_{0.5}$ system is situated in a more negative position, showing that the interactions are the strongest within this system.[33] This analysis could map the interaction regions *via* RDG isosurface with three distinct colours (blue-green-red), representing attraction, intermediate interaction and repulsion, respectively. For example, in the $(TBAC)_{0.5}(PhSeBr)_{0.5}$ system, a blue center and surrounding green disc-like RDG isosurface appeared between the Se atom and Cl^-, representing the formation of a strong ChB. Meanwhile, the Se atom and Br atom both could connect with the surrounding H atoms by HB interactions in view of their amphiphilic property, displayed as green isosurfaces (Fig. 3b). From this, it seems clear that the formed HBs are weak in this system and strong ChB interactions could be recognized as the dominant driving force. The same goes for the $(TBAC)_{0.5}(PhSeCl)_{0.5}$ system but, by contrast, a bluer center isosurface emerged between C–Se and Cl^-, showing that a much stronger ChB interaction exists in this system. For the other two systems, they both present a blue center and surrounding green RDG isosurface between C–Se and Br^-, and simultaneously there are some weak HB interactions as well (Fig. S8–S10b, ESI†). Besides, the interaction energies (E_{int}) of these eutectic solvents are comparable to the strength of some reported σ-hole interactions (Fig. S11–S14, ESI†).[34] Above all, the strong ChB interactions are key factors to drive the formation of these eutectic solvents.

Additionally, the natural orbitals for chemical valence (NOCV) analysis could further extract and directly quantify the types of chemical bonds from the orbital interactions of the fragments' points of view.[35] We could see from Fig. 3d and Fig. S8–S10d (ESI†) that the NOCV pairs of these four eutectic systems all have the largest eigenvalues between the C–Se and halogen anions of quaternary ammonium salts, which leads to electron transfer from the lone pairs of Cl^-/Br^- to the σ* antibonding orbitals of C–Se, giving a paradigm of positive and negative deformation densities along the $Cl^-/Br^-\cdots$Se–C fragment. Thus, the formation of these DESs could be ascribable to the strong ChB interactions between the components.

Conclusions

To summarize, an emerging deep eutectic solvent system dominated by the chalcogen bond interaction was presented in this work. Herein, we designed and prepared four kinds of ChB DESs as illustration. The DSC experiments, melting points and ^{13}C NMR spectra demonstrated the formation of such deep eutectic solvent systems and there were only noncovalent interactions between the components. Then, the FT-IR and UV-vis spectra further indicated the types of dominant interaction and interaction sites. The TGA analyses displayed the better thermostability of the prepared ChB DESs. Furthermore, DFT calculations were carried out to comprehend the formation mechanism as a promising additional method, and the results showed that the strong ChB interactions were the

primary driving forces that contribute to the formation of the deep eutectic solvent systems. In the future, these ChB DESs are expected to be applied in the fields of material preparation, radioactive elements capture, *etc.*

Author contributions

Ruifen Shi: investigation, writing – original draft, writing – review & editing. Zeyu Wang, Chenyang Wei, Rui Qin, investigation. Dongkun Yu, conceptualization, Tiancheng Mu: conceptualization, writing – review & editing, supervision.

Data availability

The data supporting this article have been included as part of the ESI.†

Conflicts of interest

There are no conflicts to declare.

Acknowledgements

The authors thank the National Natural Science Foundation of China (22073112) for financial support.

Notes and references

1 B. B. Hansen, S. Spittle, B. Chen, D. Poe, Y. Zhang, J. M. Klein, A. Horton, L. Adhikari, T. Zelovich, B. W. Doherty, B. Gurkan, E. J. Maginn, A. Ragauskas, M. Dadmun, T. A. Zawodzinski, G. A. Baker, M. E. Tuckerman, R. F. Savinell and J. R. Sangoro, *Chem. Rev.*, 2021, **121**, 1232–1285.
2 T. Zhang, T. Doert, H. Wang, S. Zhang and M. Ruck, *Angew. Chem., Int. Ed.*, 2021, **60**, 22148–22165.
3 A. P. Abbott, G. Capper, D. L. Davies, R. K. Rasheed and V. Tambyrajah, *Chem. Commun.*, 2003, 70–71.
4 J. Wang, C. Teng and L. Yan, *Green Chem.*, 2022, **24**, 552–564.
5 S. Liu, B. Zhang, Z. Yang, Z. Xue and T. Mu, *Green Chem.*, 2023, **25**, 2620–2628.
6 Y. Liu, N. Deak, Z. Wang, H. Yu, L. Hameleers, E. Jurak, P. J. Deuss and K. Barta, *Nat. Commun.*, 2021, **12**, 5424.
7 A. A. Quintana, A. M. Sztapka, V. D. C. Santos Ebinuma and C. Agatemor, *Angew. Chem., Int. Ed.*, 2022, **61**, e202205609.
8 R. Shi, D. Yu, F. Zhou, J. Yu and T. Mu, *Chem. Commun.*, 2022, **58**, 4607–4610.
9 W. Wang, B. Ji and Y. Zhang, *J. Phys. Chem. A*, 2009, **113**, 8132–8135.
10 P. Scilabra, G. Terraneo and G. Resnati, *Acc. Chem. Res.*, 2019, **52**, 1313–1324.
11 R. Hein, A. Docker, J. J. Davis and P. D. Beer, *J. Am. Chem. Soc.*, 2022, **144**, 8827–8836.
12 S. Benz, J. López-Andarias, J. Mareda, N. Sakai and S. Matile, *Angew. Chem., Int. Ed.*, 2017, **56**, 812–815.
13 S. Langis-Barsetti, T. Maris and J. D. Wuest, *J. Org. Chem.*, 2017, **82**, 5034–5045.
14 R. J. Fick, G. M. Kroner, B. Nepal, R. Magnani, S. Horowitz, R. L. Houtz, S. Scheiner and R. C. Trievel, *ACS Chem. Biol.*, 2016, **11**, 748–754.
15 D. O. Abranches, M. A. R. Martins, L. P. Silva, N. Schaeffer, S. P. Pinho and J. A. P. Coutinho, *Chem. Commun.*, 2019, **55**, 10253–10256.
16 D. Yu and T. Mu, *J. Phys. Chem. B*, 2019, **123**, 4958–4966.
17 D. Yu, H. Mou, H. Fu, X. Lan, Y. Wang and T. Mu, *Chem. – Asian J.*, 2019, **14**, 4183–4188.
18 Q. J. Shen and W. J. Jin, *Phys. Chem. Chem. Phys.*, 2011, **13**, 13721–13729.
19 J. S. Murray and P. Politzer, *WIREs Comput. Mol. Sci.*, 2011, **1**, 153–163.
20 K. Selvakumar and H. B. Singh, *Chem. Sci.*, 2018, **9**, 7027–7042.
21 A. J. Peloquin, J. M. McCollum, C. D. McMillen and W. T. Pennington, *Angew. Chem., Int. Ed.*, 2021, **60**, 22983–22989.
22 K. Helios, A. Pietraszko, W. Zierkiewicz, H. Wójtowicz and D. Michalska, *Polyhedron*, 2011, **30**, 2466–2472.
23 O. Kazarina, V. Agieienko, R. Nagrimanov, M. Atlaskina, A. Petukhov, A. Moskvichev, A. Nyuchev, A. Barykin and I. Vorotyntsev, *J. Mol. Liq.*, 2021, **344**, 117925.
24 B. K. Ifra, S. Sharma, A. Chaurasiya, A. K. Biswal, P. Hariprasad and S. Saha, *J. Appl. Polym. Sci.*, 2021, **138**, 50422.
25 D. I. Kochubey, P. V. Berdnikova, Z. P. Pai, Y. A. Chesalov, V. V. Kanazhevskiy and T. B. Khlebnikova, *J. Mol. Catal. A: Chem.*, 2013, **366**, 341–346.
26 T. Yamada and M. Mizuno, *ACS Omega*, 2018, **3**, 8027–8035.
27 G. E. Garrett, G. L. Gibson, R. N. Straus, D. S. Seferos and M. S. Taylor, *J. Am. Chem. Soc.*, 2015, **137**, 4126–4133.
28 L. Vogel, P. Wonner and S. M. Huber, *Angew. Chem., Int. Ed.*, 2019, **58**, 1880–1891.
29 R. Zeng, Z. Gong, L. Chen and Q. Yan, *ACS Macro Lett.*, 2020, **9**, 1102–1107.
30 E. R. Johnson, S. Keinan, P. Mori-Sánchez, J. Contreras-García, A. J. Cohen and W. Yang, *J. Am. Chem. Soc.*, 2010, **132**, 6498–6506.
31 M. Ranjbar, A. Nowroozi, E. J. C. Nakhaei and T. Chemistry, *Comput. Theor. Chem.*, 2022, **1216**, 113867.
32 K. Biernacki, H. i K. Souza, C. u M. Almeida, A. L. Magalhães and M. P. Gonçalves, *ACS Sustainable Chem. Eng.*, 2020, **8**, 18712–18728.
33 M. Ranjbar, A. Nowroozi and E. Nakhaei, *Comput. Theor. Chem.*, 2022, **1216**, 113867.
34 G. R. Desiraju, *Acc. Chem. Res.*, 2002, **35**, 565–573.
35 M. P. Mitoraj and A. Michalak, *J. Mol. Model.*, 2013, **19**, 4681–4688.